Enhancement of squeezing in resonance fluorescence of a driven quantum dot close to a graphene sheet

Wei Fang, Qing-lin Wu, Shao-ping Wu, and Gao-xiang Li*
Department of Physics, Huazhong Normal University, Wuhan 430079, P.R. China
(Received 3 March 2016; published 24 May 2016)

We investigate squeezing of the resonance fluorescence of a laser-driven quantum dot (QD) close to a graphene sheet. The coupling between the QD and the surface plasmon around the graphene sheet is frequency dependent in the terahertz region, which can be adjusted by the laser intensity. Distinct decay rates in different transition channels of dressed QDs can be achieved due to the tailored photon reservoir, which can be used to improve the squeezing. It is found that increases in both the dephasing rate and the environmental temperature are harmful to the squeezing. Meanwhile, an enhancement in the QD-plasmon coupling strength may reduce the fragility of squeezing against the decoherence process. Additionally, in the strong light-matter coupling region, squeezing can be largely enhanced by tuning the strength of the pump field and its detuning from the QD.

DOI: 10.1103/PhysRevA.93.053831

I. INTRODUCTION

Graphene is a thin layer of carbon atoms bonded in a hexagonal structure and arranged in a honeycomb crystal lattice [1,2]. Due to its peculiar optical properties, it has been extensively investigated both theoretically and experimentally [3–9]. It has been reported that graphene can support different kinds of surface waves in the terahertz (THz) region [10], which can be attributed to the collective excitations of electrons around the surface. The surface wave often possesses an extremely high local density of states (LDOS), restricted near the graphene's surface and termed the surface plasma field (SPF) [11–15]. In the THz region, the conductivity of graphene can be described as Kubo formations [16]. In more detail, the optical property of graphene is often connected to intraband and interband interactions [17–22], which dominate the real part and the imaginary part of the conductivity in the low-temperature limit, respectively. Unlike normal two-dimensional materials, graphene possesses a tunable conductivity, which can be affected by controlling the environmental temperature or the ac electric field added to it or by applying different chemical doping methods [23–27]. The tunability of the conductivity originates from the high mobility of the carrier concentration [28,29]. It has been reported that the Fermi energy of graphene will suffer a change when a static electric field is added [27,30]. That is, the conducting channels of electron-hole gases will shift, which causes a different optical response of the graphene sheet to an incident light beam [31,32]. This tunable property, together with its low loss and the easily achieved experimental conditions, ensures that graphene can significantly modify the electromagnetical property around it.

It is known that the power spectrum of a coherent driven two-level quantum emitter can exhibit a splitting Mollow triplet [33] because the inelastic scattering originates from the strong coupling between the driving field and the emitter [34]. In 1981, Zoller *et al.* proposed that the quantum fluctuations of the radiation field produced by the laser-driven qubit can be squeezed below the quantum vacuum limit [35]. Potential applications of the squeezing field in various areas have been investigated, such as gravitational wave detection [36], quantum teleportation [37], and quantum computing [38]. Recently, the observation of squeezing in resonance fluorescence has been realized by the use of a large dipole artificial atom [39]. Also, the atom's ensembles [40–42] are designed to easily obtain single-mode and multimode squeezed light. Agio *et al.* [43] studied the radiation spectrum of a single quantum emitter placed adjacent to a gold nanosphere. Owing to the strong scattering effect of the nanostructure, even in the far-field region, the squeezing intensity can show a prominent enhancement. Additionally, the strong coupling between the emitter and the SPF on the golden ball weakens the destructive influence of the dephasing process on squeezing, thus squeezing can be easily obtained. It has been shown that when the coherence of the emitter is perfectly under control, optimal squeezing of resonance fluorescence can be achieved [44,45]. Large squeezing in the spectrum can be expected when one transition channel of the dressed QD is deeply suppressed while the other transition channel is enhanced [46]. For a quantum system consisting of a QD and a graphene sheet, it is feasible to modulate the coupling between the emitter and the SPF by changing the Fermi energy of graphene, which is easy to realize experimentally [8,27,30].

In this paper, we investigate the radiation properties of a laser-driven QD situated near a graphene sheet. We present a detailed treatment of the influence of graphene's Fermi energy, the dephasing process of the QD, the Rabi frequency, and the coupling of the driven QD with the SPF on squeezing. By use of the Green function of the electromagnetic field around the graphene sheet, the Purcell factor is studied to illustrate the interaction between the quantum system and graphene. After diagnolizing the laser-dot interaction, the master equation and the corresponding Bloch equations are derived in the dressed-state basis. Aside from numerical calculations, the approximated analytical expression of the spectrum is also given. It is shown that the conditions for achieving squeezing can be largely relaxed when the QD couples strongly with the SPF around the graphene. However, it is easy to generate squeezing with a lower temperature and weaker decoherence process in the strong QD-SPF coupling region. When the QD interacts strongly with the SPF, squeezing can be enhanced by choosing the relevant parameters of the pump field or adjusting the Fermi energy of graphene.

*gaox@phy.ccnu.edu.cn

The paper is organized as follows. In Sec. II we introduce the model and derive the Green function in the upper half-space, then the Purcell factor is studied and the explicit form of the master equation for a dressed QD is acquired. Section III presents the noise spectra versus the dephasing rates, QD-graphene distances, and environmental temperatures. In Sec. IV the influence of the Fermi energy on squeezing is studied. Also, the decay rates of dressed QDs through different transition channels are plotted to express the importance of an unbalanced transition process in the generation of squeezed light. Finally, a summary is given in Sec. V.

II. COUPLING BETWEEN QUANTUM DOT AND RESERVOIR

The system under consideration consists of a two-level QD with ground state $|g\rangle$ and excited state $|e\rangle$, driven by a monochromatic laser field and coupled to a suspended graphene sheet, as shown in Fig. 1. The graphene sheet is placed in the x-y plane and the QD is distance d from it, with coordinate $\mathbf{r}_d = (0,0,z_0)$. The excitation frequency of the QD is denoted ω_0 and located in the terahertz region [47–49]; here we take $\omega_0 = 125$ meV. The dipole moment ($\mathbf{p} = 50$ D) of the QD is modeled in the point dipole approximation and vertical to the graphene sheet, where the polarization of the pump laser is aligned with the dipole moment and has the central frequency ω_l. Then the Hamiltonian of the system can be given as

$$H = \int d^3\mathbf{r} \int \hbar\omega \hat{\mathbf{f}}^\dagger(\mathbf{r},\omega)\hat{\mathbf{f}}(\mathbf{r},\omega)d\omega + \frac{\hbar\Omega}{2}(\hat{\sigma}_+ e^{-i\omega_l t} + \text{H.c.}) + \frac{\hbar\omega_0}{2}\hat{\sigma}_z - \left[\hat{\sigma}_+ \int \mathbf{p}\cdot\hat{\mathbf{E}}^{(+)}(\mathbf{r}_d,\omega)d\omega + \text{H.c.}\right]. \quad (1)$$

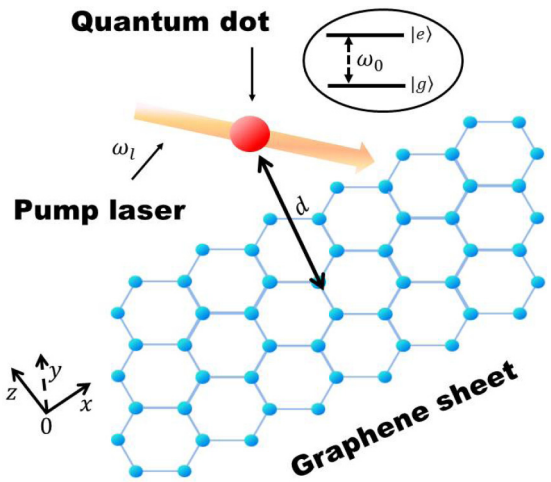

FIG. 1. Geometry of the system. The z axis is taken normal to the graphene sheet with its origin located on the surface, and the QD is situated in the upper space at a distance d above the graphene, with a z-polarized dipole and excitation frequency ω_0, which corresponds to the transition between the excited state $|e\rangle$ and the ground state $|g\rangle$. A classical laser beam, whose polarization is assumed to be parallel to the dipole momentum of the QD, has central frequency ω_l and acts as the pump field.

The QD is described by the Pauli operators $\hat{\sigma}_-$ and $\hat{\sigma}_+$ that satisfy the commutation relation $[\hat{\sigma}_-,\hat{\sigma}_+] = -\hat{\sigma}_z$. The basic bosonic operators $\hat{\mathbf{f}}^\dagger(\mathbf{r},\omega)$ and $\hat{\mathbf{f}}(\mathbf{r},\omega)$ represent the creation and annihilation of a polariton in the reservoir [50] and have the commutation relation $[\hat{\mathbf{f}}(\mathbf{r},\omega),\hat{\mathbf{f}}^\dagger(\mathbf{r}',\omega')] = \delta(\mathbf{r}-\mathbf{r}')\delta(\omega-\omega')$. The parameter Ω is the Rabi frequency of the driven system, which also denotes the interaction strength between the QD and the pump field. The vector $\mathbf{r}_d$ indicates the location of the QD, while the electric-field operator $\hat{\mathbf{E}}^{(+)}(\mathbf{r}_d,\omega)$ mediates the field at the same spacial point under the dipole approximation and has the form [51]

$$\hat{\mathbf{E}}^{(+)}(\mathbf{r}_d,\omega) = i\frac{\omega^2}{c^2}\int d\mathbf{r}\sqrt{\frac{\text{Im}[\varepsilon(\mathbf{r},\omega)]\hbar}{\pi\varepsilon_0}}\overleftrightarrow{\mathbf{G}}(\mathbf{r}_d,\mathbf{r},\omega)\cdot\hat{\mathbf{f}}(\mathbf{r},\omega). \quad (2)$$

The permittivity of graphene is denoted $\varepsilon(\mathbf{r},\omega)$ and $\text{Im}[\varepsilon(\mathbf{r},\omega)]$ represents its imaginary part. The propagating Green function $\overleftrightarrow{\mathbf{G}}(\mathbf{r}_d,\mathbf{r},\omega)$ of the field is introduced to illustrate the electromagnetic response at $\mathbf{r}_d$ due to an excitation at $\mathbf{r}$ and satisfies the equation $[\nabla\times\mu^{-1}(\mathbf{r},\omega)\nabla\times - \omega^2/c^2\varepsilon(\mathbf{r},\omega)]\overleftrightarrow{\mathbf{G}}(\mathbf{r},\mathbf{r}',\omega) = \overleftrightarrow{\mathbf{I}}\,\delta(\mathbf{r}-\mathbf{r}')$. In this expression, $\overleftrightarrow{\mathbf{I}}$ is unit dyadic and $\delta(\mathbf{r}-\mathbf{r}')$ depicts a point source at position $\mathbf{r}'$ [52]. After applying the plane-wave expansion method and taking the boundary conditions into account, the Green function can be explicitly written as [53]

$$\overleftrightarrow{\mathbf{G}}(\mathbf{r},\mathbf{r}',\omega) = \frac{i}{4\pi}\int d^2\mathbf{k}\frac{\mu_0}{\beta_0}\sum_{q=p,s}\zeta_q\Big[r^q_{v\to g}\mathbf{e}^+_q\mathbf{e}^-_q e^{i\beta_0(z+z')} + \mathbf{e}^-_q\mathbf{e}^-_q e^{-i\beta_0(z-z')}\Theta(z'-z) + \mathbf{e}^+_q\mathbf{e}^+_q e^{i\beta_0(z-z')}\Theta(z-z')\Big]e^{i\mathbf{k}\cdot(\boldsymbol{\rho}-\boldsymbol{\rho}')}. \quad (3)$$

Here $\mathbf{k}$ and β_0 are the parallel and vertical components of the wave vector; the index 0 is used to denote the physical quantities in a vacuum. The orthonormal polarization vectors $\mathbf{e}^\pm_p = (\mp\beta_0\mathbf{k} + k\mathbf{z})/k_0$ and $\mathbf{e}^\pm_s = \mathbf{k}\times\mathbf{z}$ indicate different propagating directions of the electromagnetic waves in the upper space. $\Theta(z)$ is the unit step function, $\zeta_p = 1$, $\zeta_s = -1$, and $r^q_{v\to g}$ is the reflection coefficient of the vacuum-graphene interface. In our case the dipole moment of the QD is perpendicular to the graphene sheet, which indicates that only a TM (p) polarized wave can be excited. Thus q can be simply replaced with p in the Green function. The reflection coefficient of the interface can be derived by following the Fresnel reflection theory and appears to be

$$r_{v\to g} = \frac{\sigma(\omega,\mu,T)\beta_0}{\sigma(\omega,\mu,T)\beta_0 - 2\omega\varepsilon_0}. \quad (4)$$

The optical response of structures made of graphene has been investigated widely, and it is known that a graphene sheet can be represented by an infinitesimally thin, two-sided surface characterized by the surface conductivity $\sigma(\omega,\mu,T)$ [54,55].

The detailed formation can be derived through the Kubo theory [16],

$$\sigma(\omega,\mu_f,T) = \frac{ie^2k_BT}{\pi\hbar^2(\omega+i\gamma_a)}\left[\frac{\mu_f}{k_BT}+2\ln(e^{-\mu_f/k_BT}+1)\right] + \frac{ie^2(\omega+i\gamma_b)}{4\pi}\int_0^\infty \frac{d_f(\eta)-d_f(-\eta)}{\eta^2-\hbar^2(\omega+i\gamma_b)^2/4}d\eta, \quad (5)$$

where e is the charge of the electron, k_B is the Boltzmann constant, T is the environmental temperature, and $d_f(\eta) = 1/(e^{(\eta-\mu_f)/k_BT}+1)$ is the Femi-Dirac distribution function. The Fermi energy of the graphene is denoted μ_f and can be modulated by changing the bias voltage. The first and second terms in the conductivity are due to the intraband and interband contributions, respectively. Coefficients γ_a and γ_b are the scattering rates due to intraband and interband transitions, which often relate to the impurities of graphene. Practically, the scatter through the interband only broadens the transition width and does not affect the main physics [27,56]; thus we take γ_b equal to 0 for convenience. It has been proven that when a photon's energy is low, interband transitions are blocked due to the existence of electrons and holes near the band edges [18,21]. In the meantime, intraband transitions exhibit Drude-like behavior and make a dominant contribution in the transmission of the SPF [57]. Experimentally, measured values of the intraband scattering time range from femoseconds to several picoseconds [20,58,59]; in this paper we use $\gamma_a = 1$ ps^{-1} and $\gamma_a = 3.3$ ps^{-1} for the zero-temperature and room-temperature cases, respectively.

It is known that in free space, the density of states of the electromagnetic field is proportional to the imaginary part of the Green function [60]. The free-space Green function can be acquired by eliminating the boundary conditions in Eq. (3) and its imaginary part turns out to be $\mathrm{Im}G_{0zz}(\mathbf{r}_d,\mathbf{r}_d,\omega) = \omega/6\pi c$. The Purcell factor is the usual measurement to judge the enhancement of the dipole decay rates (or the LDOS of the electromagnetic field) due to the different electromagnetic response resulting from the appearance of materials. Its value is determined by the ratio of the material-induced emission rate to the free-space decay rate [61,62], and here we use R to denote it. As mentioned above, graphene can support the SPF in the THz region. In Fig. 2 we plot the Purcell factor (R) for different Fermi energies and environmental temperatures. It is shown that for $\mu_f = 90$ meV, the coupling strength between the QD and the SPF approximately exhibits a Lorentzian-like shape, whereas in the zero-temperature case the curve has a higher peak and narrower half-width. In the inset, the case $\mu_f = 120$ meV is studied for comparison. Obviously for a higher Fermi energy, the resonant frequency of the SPF suffers a blue shift and the maximum value of the Purcell factor decreases. Upon comparing the results in Figs. 2(a) and 2(b), it is clear that when the QD is closer to the graphene sheet, the increase in the LDOS is more prominent. On the contrary, the Purcell factor tends to be distributed averagely in the frequency for a large QD-graphene distance. The different behaviors of the Purcell factor reflect the fact that, owing to the high locality of the SPF, a small QD-graphene distance will result in strong light-matter coupling. Additionally, it can be predicted that for a quantum system with a fixed transition frequency, one

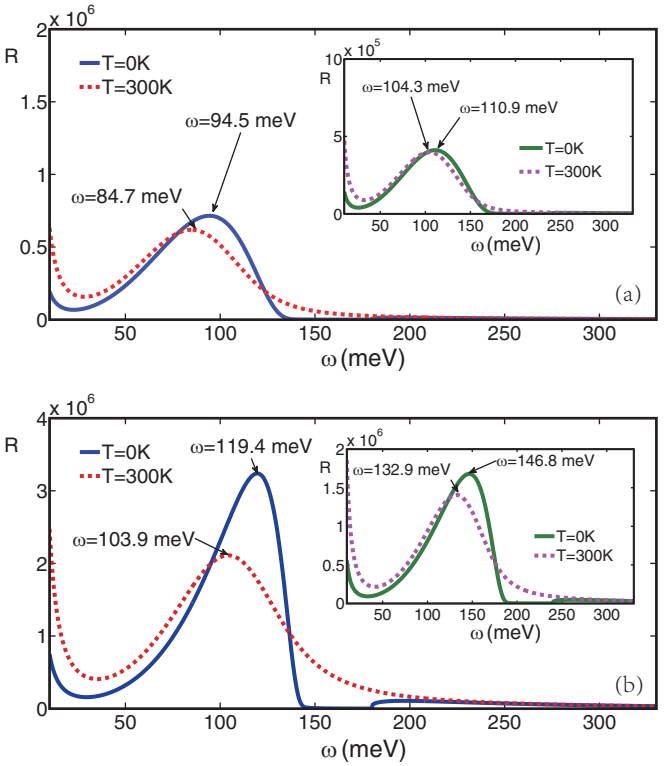

FIG. 2. The Purcell factor vs the frequency. The case $\mu_f = 90$ meV at different environmental temperatures, $T = 0$ K (solid blue line) and $T = 300$ K (dashed red line), is considered. Inset: The case $\mu_f = 120$ meV, at environmental temperatures of $T = 0$ K (solid green line) and $T = 300$ K (dashed pink line), is considered in comparison to the former case. Locations of peaks are shown by arrows, and different QD-graphene distances are investigated: (a) $d = 20$ nm; (b) $d = 10$ nm.

can modulate the decay process by building a strong coupling between the QD and the SPF, which is important in producing squeezing and is discussed in Sec. IV.

Note that the dispersion relation for an SPF propagating along the graphene sheet can be solved by finding the pole(s) of the reflection coefficient $r_{v\to g}$ in Eq. (3) [63,64], and the scattered Green function can be written by the combination of two parts: the discrete SPF modes plus the integral over the continuum of radiation modes that is located in the proper branch cut. Additionally, it has been pointed out that loss of material may dominate the decay process when the emitter is close to the graphene sheet [6]. Thus before proceeding to study the radiation properties of the system, we first investigate the Purcell factor versus the QD's position to check the validity of the parameters chosen, which is illustrated in Fig. 3. As depicted in the figure, for the working frequency of the QD, $\omega_0 = 125$ meV (the relevant vacuum wavelength is $\lambda_0 = 10$ μm), and the Fermi energy of graphene, $\mu_f = 90$ meV, the SPF dominates the QD decay when the QD is placed at a distance of about $10^{-3}\lambda_0$ (several nanometers to tens of nanometers) above the graphene sheet. The case where $\mu_f = 120$ meV is also plotted for comparison. It is shown that the SPF still makes a dominant contribution in the same region; only a subtle decrease in the Purcell factor can be observed. The circumstances are similar at room temperature, thus for

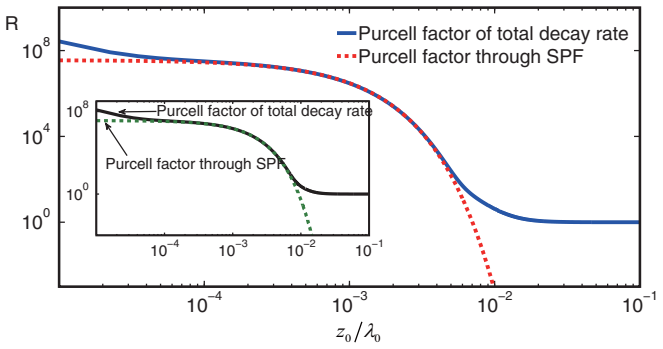

FIG. 3. The Purcell factor vs the QD's position. The case where $\mu_f = 90$ meV and $T = 0$ K at the QD's excitation frequency is investigated, both the enhancement of the total decay rate (solid blue line) and the decay through SPF (dashed red line) are plotted. Inset: The case where $\mu_f = 120$ meV at the same temperature.

the QD-graphene distance we choose ($d = 10$ and 20 nm); the QD couples strongly with the SPF modes.

We now proceed to deduce the master equation of the dressed QD. In a frame rotating at the laser's frequency ω_l, the Hamiltonian of the system takes the form

$$H = H_{DS} + H_I, \tag{6}$$

$$H_{\rm DS} = \frac{1}{2}[\hbar\Delta\hat{\sigma}_z + \hbar\Omega(\hat{\sigma}_+ + \hat{\sigma}_-)], \tag{7}$$

$$H_I = -\left[\hat{\sigma}_+ \int \mathbf{p}\cdot\hat{\mathbf{E}}^{(+)}(\mathbf{r}_d,\omega)e^{i(\omega_l-\omega)t}d\omega + \text{H.c.}\right], \tag{8}$$

where $\Delta = \omega_0 - \omega_l$ is the detuning of the QD excitation frequency from the driving-field frequency, $H_{\rm DS}$ is the Hamiltonian of driven system, and H_I describes the interaction between the QD and the reservoir. Then second-order perturbation theory is applied by tracing over the reservoir degrees of freedom through [65]

$$\frac{\partial\tilde{\rho}}{\partial t} = -\frac{1}{h^2}\int_0^t \text{Tr}_{\rm R}\{[\tilde{H}_I(t),[\tilde{H}_I(t-\tau),\tilde{\rho}(t-\tau)]]\}d\tau. \tag{9}$$

Under the Born-Markovian approximation, the operator $\tilde{\rho}(t-\tau)$ can be replaced with $\tilde{\rho}(t)\otimes\tilde{\rho}_R(0)$, where $\tilde{\rho}(t)$ is the reduced density operator for the dressed QD, $\tilde{\rho}_R(0)$ is the initial reservoir operator, and $\text{Tr}_{\rm R}$ denotes tracing over the reservoir variables. The bath is described by $\text{Tr}_{\rm R}[\hat{\mathbf{f}}(\mathbf{r},\omega)\hat{\mathbf{f}}^\dagger(\mathbf{r}',\omega')] = [\bar{n}(\omega)+1]\delta(\mathbf{r}-\mathbf{r}')\delta(\omega-\omega')$ and $\text{Tr}_{\rm R}[\hat{\mathbf{f}}^\dagger(\mathbf{r},\omega)\hat{\mathbf{f}}(\mathbf{r}',\omega')] = \bar{n}(\omega)\delta(\mathbf{r}-\mathbf{r}')\delta(\omega-\omega')$, where $\bar{n}(\omega) = 1/(e^{\hbar\omega/k_BT}-1)$ represents the average excitation number of the reservoir. After straightforward calculation, the master equation for the reduced density operator of the driven QD proves to be

$$\begin{aligned}\frac{d\rho}{dt} =& \frac{1}{i\hbar}[H_{\rm DS},\rho] + \int_0^\infty d\omega\gamma^{\bar{n}+1}(\mathbf{r}_d,\omega)\int_0^t d\tau\{e^{-i(\omega-\omega_l)\tau}\\ &\times[\hat{\sigma}_-(-\tau)\rho\hat{\sigma}_+ - \hat{\sigma}_+\hat{\sigma}_-(-\tau)\rho] + \text{H.c.}\}\\ &+ \int_0^\infty d\omega\gamma^{\bar{n}}(\mathbf{r}_d,\omega)\int_0^t d\tau\{e^{i(\omega-\omega_l)\tau}[\hat{\sigma}_+(-\tau)\rho\hat{\sigma}_-\\ &- \hat{\sigma}_-\hat{\sigma}_+(-\tau)\rho] + \text{H.c.}\} + \mathcal{L}_p.\end{aligned} \tag{10}$$

In the above equation the first term interprets the coherent evolution of the driven QD, whereas the remaining terms represent the reservoir-induced decay processes. It should be pointed out that the damping coefficients, denoted $\gamma^{\bar{n}+1}(\mathbf{r}_d,\omega) = [\bar{n}(\omega)+1]\mathbf{p}\cdot\text{Im}\overleftrightarrow{\mathbf{G}}(\mathbf{r}_d,\mathbf{r}_d,\omega)\cdot\mathbf{p}\omega^2/c^2\pi\hbar\varepsilon_0$ and $\gamma^{\bar{n}}(\mathbf{r}_d,\omega) = \bar{n}(\omega)\mathbf{p}\cdot\text{Im}\overleftrightarrow{\mathbf{G}}(\mathbf{r}_d,\mathbf{r}_d,\omega)\cdot\mathbf{p}\omega^2/c^2\pi\hbar\varepsilon_0$, represent the reservoir-assisted decay rates of the QD. Since we focus on the THz operation, in the far-infrared frequency region (0.3–6 THz) the thermal average excitation number may be large at a nonzero environmental temperature, thus we do not neglect the contribution of $\bar{n}(\omega)$ as usually done. Practically, the dephasing process has been simply taken into account by introducing the damping term $\mathcal{L}_p = \gamma_0(2\hat{\sigma}_{ee}\rho\hat{\sigma}_{ee} - \hat{\sigma}_{ee}\hat{\sigma}_{ee}\rho - \rho\hat{\sigma}_{ee}\hat{\sigma}_{ee})/2$, where γ_0 is the dephasing rate of the QD [48,66]. The time-dependent QD operators can be expressed as $\hat{\sigma}_\pm(\tau) = \alpha^2\tilde{\sigma}_\pm e^{\pm i\bar{\Omega}\tau} - \beta^2\tilde{\sigma}_\mp e^{\mp i\bar{\Omega}\tau} + \alpha\beta\tilde{\sigma}_z$, where $\bar{\Omega} = \sqrt{\Omega^2+\Delta^2}$ is the energy difference between the upper dressed state $|+\rangle = \alpha|g\rangle + \beta|e\rangle$ and the lower dressed state $|-\rangle = \beta|g\rangle + \alpha|e\rangle$, with $\alpha = \sqrt{(1+\Delta/\bar{\Omega})/2}$ and $\beta = \sqrt{(1-\Delta/\bar{\Omega})/2}$. In the dressed-state basis $|\pm\rangle$, the Pauli operators are defined as

$$\tilde{\sigma}_+ = |+\rangle\langle-|, \tilde{\sigma}_- = |-\rangle\langle+|, \tag{11}$$

$$\tilde{\sigma}_z = |+\rangle\langle+| - |-\rangle\langle-| = \tilde{\sigma}_{++} - \tilde{\sigma}_{--}. \tag{12}$$

III. SQUEEZING SPECTRUM OF RESONANCE FLUORESCENCE RADIATED BY A DRIVEN QUANTUM DOT

The in-phase quadrature of a normally ordered noise spectrum emitted by a driven QD can be expressed in terms of two-time correlations of the QD operators, which have the form [67]

$$\begin{aligned}S_x(\omega) =& \text{Re}\int_0^\infty d\tau\cos(\Delta\omega\tau)\lim_{t\to\infty}[\langle\sigma_+(t+\tau),\sigma_-(t)\rangle\\ &+ \langle\sigma_-(t+\tau),\sigma_-(t)\rangle].\end{aligned} \tag{13}$$

The squeezing spectrum of resonance fluorescence takes place only when $S_x(\omega)$ is negative. In Fig. 4 we study the spectrum of the driven system at zero temperature for different dephasing rates, QD-laser detunings, and QD-graphene distances. The Fermi energy of graphene and the Rabi frequency are taken to be 90 and 20 meV, respectively. It is shown that when the QD is placed 20 nm above the graphene sheet and the detuning is 25 meV, squeezing of the spectrum only occurs for the lower dephasing rate, which is depicted by the solid purple line in Fig. 4(a). Figure 4(b) displays the stronger coupling case where the QD-graphene distance decreases to 10 nm; apparently, squeezing can be produced even for an extremely high dephasing rate ($\gamma_0 = 0.1$ meV). However, the dephasing process has a destructive effect on squeezing (dashed green line). For smaller QD-graphene distances, the increase in the coupling strength between the QD and the SPF leads to an enhancement of squeezing, which is directly shown by the discrepancy in the amplitudes between the sidebands and the central peak.

The physics associated with the coherent driven transition system can be clearly explored by working in the dressed-state basis [68]. Moreover, when the pump field is strong enough

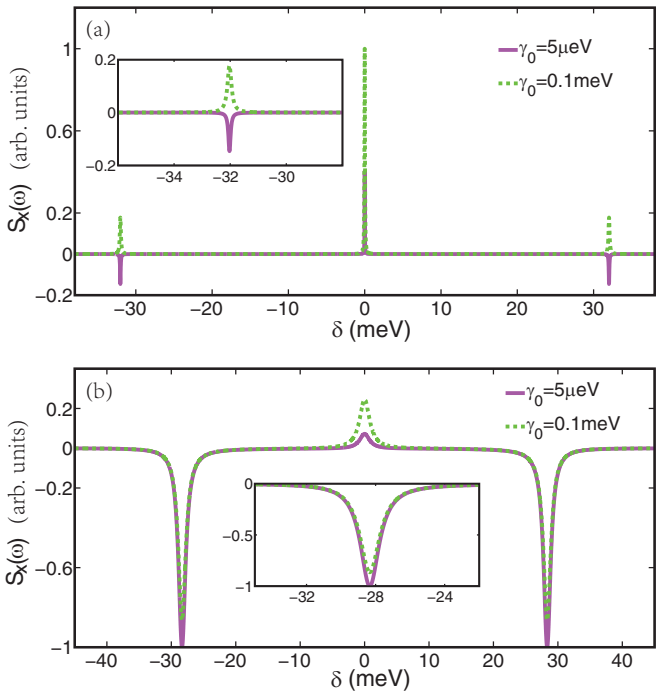

FIG. 4. Noise spectrum of the fluorescence field for $\mu_f = 90$ meV, $\Omega = 20$ meV, $T = 0$ K, and (a) $d = 20$ nm and $\Delta = 25$ meV or (b) $d = 10$ nm and $\Delta = 20$ meV. The solid purple line represents the weaker-dephasing-rate case ($\gamma_0 = 5$ μeV) and the dashed green line represents the stronger-dephasing case ($\gamma_0 = 0.1$ meV).

($\bar{\Omega} \gg \gamma^{\bar{n}+1}, \gamma_0$), the secular approximation is valid. Then the simplified Bloch equations appear to be

$$\langle \dot{\tilde{\sigma}}_+ \rangle = (i\bar{\Omega} - \Gamma_p)\langle \tilde{\sigma}_+ \rangle, \tag{14}$$

$$\langle \dot{\tilde{\sigma}}_- \rangle = -(i\bar{\Omega} + \Gamma_p)\langle \tilde{\sigma}_- \rangle, \tag{15}$$

$$\langle \dot{\tilde{\sigma}}_z \rangle = -\Gamma_i \langle \tilde{\sigma}_z \rangle + \Gamma'. \tag{16}$$

Here Γ_i and Γ_p represent the decay rates of population inversion and polarization in the dressed state. The relations $\Gamma_i = \Gamma_- + \Gamma_+$ and $\Gamma' = \Gamma_- - \Gamma_+$ have been used in the derivation of the above equations, where Γ_+ represents the transition rate from the upper dressed state $|+\rangle$ to the lower dressed state $|-\rangle$ and Γ_- denotes the transition rate from $|-\rangle$ to $|+\rangle$. Through the definitions $\omega_l^+ = \omega_l + \bar{\Omega}$ and $\omega_l^- = \omega_l - \bar{\Omega}$, detailed expressions of the decay rates have the following forms:

$$\Gamma_+ = 2\pi\alpha^4\gamma^{\bar{n}+1}(\omega_l^+) + 2\pi\beta^4\gamma^{\bar{n}}(\omega_l^-) + \alpha^2\beta^2\gamma_0, \tag{17}$$

$$\Gamma_- = 2\pi\beta^4\gamma^{\bar{n}+1}(\omega_l^-) + 2\pi\alpha^4\gamma^{\bar{n}}(\omega_l^+) + \alpha^2\beta^2\gamma_0, \tag{18}$$

$$\begin{aligned}\Gamma_p =& \pi\alpha^4[\gamma^{\bar{n}+1}(\omega_l^+) + \gamma^{\bar{n}}(\omega_l^+)] + \pi\beta^4[\gamma^{\bar{n}+1}(\omega_l^-) \\ &+ \gamma^{\bar{n}}(\omega_l^-)] + 4\pi\alpha^2\beta^2[\gamma^{\bar{n}+1}(\omega_l) + \gamma^{\bar{n}}(\omega_l)] \\ &+ (\alpha^4 + \beta^4)\gamma_0/2.\end{aligned} \tag{19}$$

Starting from Eqs. (14)–(16), the analytical form of the noise spectrum, which can be derived by means of the quantum regression theory [69], turns out to be

$$\begin{aligned}S_x(\omega) =& \frac{\Gamma_p}{4\bar{\Omega}}\left[\frac{\Delta^2}{\bar{\Omega}} + (\langle\tilde{\sigma}_{++}\rangle_{ss} - \langle\tilde{\sigma}_{--}\rangle_{ss})\Delta\right] \\ &\times\left[\frac{1}{\Gamma_p^2 + (\delta\omega + \bar{\Omega})^2} + \frac{1}{\Gamma_p^2 + (\delta\omega - \bar{\Omega})^2}\right] \\ &+ \left(\frac{\Omega}{\bar{\Omega}}\right)^2 \frac{2\Gamma_i\langle\tilde{\sigma}_{--}\rangle_{ss}\langle\tilde{\sigma}_{++}\rangle_{ss}}{\Gamma_i^2 + \delta\omega^2},\end{aligned} \tag{20}$$

where $\langle\tilde{\sigma}_{++}\rangle_{ss}$ and $\langle\tilde{\sigma}_{--}\rangle_{ss}$ represent the stationary population distribution of the upper and lower dressed states, with the detailed forms $\langle\tilde{\sigma}_{--}\rangle_{ss} = \Gamma_+/\Gamma_i$ and $\langle\tilde{\sigma}_{++}\rangle_{ss} = \Gamma_-/\Gamma_i$, and $\langle\tilde{\sigma}_z\rangle_{ss} = \langle\tilde{\sigma}_{++}\rangle_{ss} - \langle\tilde{\sigma}_{--}\rangle_{ss} = \Gamma'/\Gamma_i$ represents the population difference between the two dressed levels. Apparently, the appearance of squeezing requires a stationary imbalanced distribution between two dressed states $|\pm\rangle$. Through Eq. (20) it is clear that the condition for squeezing lies at $\langle\tilde{\sigma}_z\rangle_{ss} < -\Delta/\bar{\Omega}$ for positive QD detuning or $\langle\tilde{\sigma}_z\rangle_{ss} > -\Delta/\bar{\Omega}$ for negative detuning. Thus according to the solution of the population difference $\langle\tilde{\sigma}_z\rangle_{ss}$, it can be concluded that the imbalanced transition process is the prominent factor in the generation of squeezing. Morever, aside from the coupling between the QD and the SPF, squeezing can also be modified by tuning the pump laser.

In Fig. 5, we investigate the population difference of the driven system for the same parameters used in Fig. 4. Figure 5(a) displays the population difference versus the QD detunings for $d = 20$ nm. It is shown that when the pump

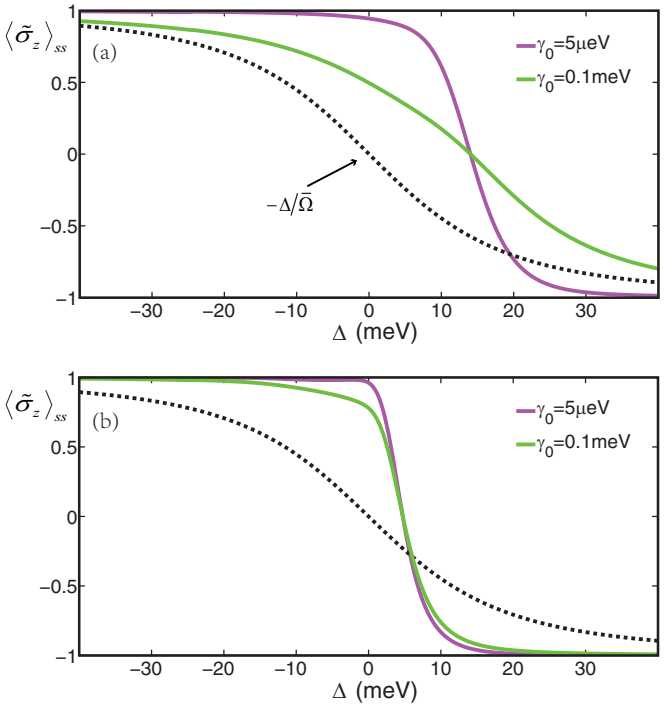

FIG. 5. Population difference $\langle\tilde{\sigma}_z\rangle$ vs detuning for $\mu_f = 90$ meV, $\Omega = 20$ meV, $T = 0$ K, and (a) $d = 20$ nm or (b) $d = 10$ nm. Different dephasing rates, $\gamma_0 = 5$ μeV (solid purple line) and $\gamma_0 = 0.1$ meV (solid green line), are considered; the dashed black line denotes the values of $-\Delta/\bar{\Omega}$.

frequency is higher than the QD's excitation frequency, i.e., the detuning is negative, squeezing can be generated at both dephasing rates. The physics can be understood with the help of Fig. 2 and the analytical solution of the spectrum. Obviously the Purcell factor at frequency $\omega_l + \bar{\Omega}$ is much smaller than the value at frequency $\omega_l - \bar{\Omega}$, which results in a high decay rate $\gamma^{\bar{n}+1}(\omega_l^-)$.That is, the transition from $|+\rangle$ to $|-\rangle$ is enhanced, while the other channel, from $|-\rangle$ to $|+\rangle$, is suppressed. As a result, the population difference has been increased. The circumstance is different when the detuning is positive. In this case, the LDOSs near the frequencies related to both transition channels, $|+\rangle \to |-\rangle$ and $|-\rangle \to |+\rangle$, are low. Therefore, the corresponding reservoir-assisted decay rates are suppressed and the total decay rates become sensitive to the dephasing process. As the figure depicts, the population difference for a high dephasing rate is not huge enough to produce squeezing, while the relevant spectrum is displayed by the dashed green line in Fig. 4(a). When the dephasing process is weak, squeezing can be generated by reasonably tuning the frequency of the pump field. As the solid purple line indicates, the population difference is huge enough to produce squeezing when the detuning is larger than 20 meV. Thus for $\Delta = 25$ meV and $\gamma_0 = 5$ μeV, squeezing of the resonance fluorescence can be observed, as shown in Fig. 4(a). Figure 5(b) depicts the case where $d = 10$ nm. Obviously the population difference shows a prominent increase, and squeezing can be easily generated in the strong-coupling region. The physics can be followed by combining the results in Fig. 2. As it depicts, the Purcell factor has a higher peak when the QD is closer to the graphene sheet, and the imbalance of decay rates originates from different transition channels becoming larger. It is obvious that when the detuning is $\Delta = 20$ meV, the population differences for both dephasing rates are sufficiently large to generate squeezing, and the corresponding spectrum is shown in Fig. 4(b).

To summarize, it is shown that the generation of squeezing depends on the dephasing rate, the detuning, and the distance between the QD and the graphene sheet. The dephasing rate has a distinct influence on squeezing since it is relevant to the decay between two dressed levels, which can be illustrated by Eqs. (17) and (18). When the dephasing process is much weaker compared to the coupling strength between QD and SPF, i.e., $\gamma^{\bar{n}+1}(\omega_l^{\pm}) \gg \gamma_0$, its influence can be neglected. Otherwise, if the dephasing process is comparable to the coupling strength, squeezing would strongly depend on the value of the dephasing rate. For example, when the dephasing process is strong enough that the QD-graphene coupling can be neglected, it is obvious that different transition channels decay at the same rate $\Gamma_+ \approx \Gamma_-$. Thus the population would tend to have a balanced distribution in the upper and lower dressed states, and no squeezing could be produced. Practically, to generate squeezed light for a high dephasing rate, enhancing the coupling strength is an efficient method. As Fig. 5(b) displays, the population difference is greatly increased in the case where $d = 10$ nm, indicating that an enhancement in the QD-graphene coupling could overcome the destructive effect caused by the dephasing process. Moreover, since the LDOS is much higher around the resonant frequency of the SPF, one could modulate the transition rates of different decay channels by tuning the pump field. When the decay channel corresponds to the transition frequency $\omega_l \pm \bar{\Omega}$ is enhanced, while the other channel is deeply suppressed, and squeezing can be obtained.

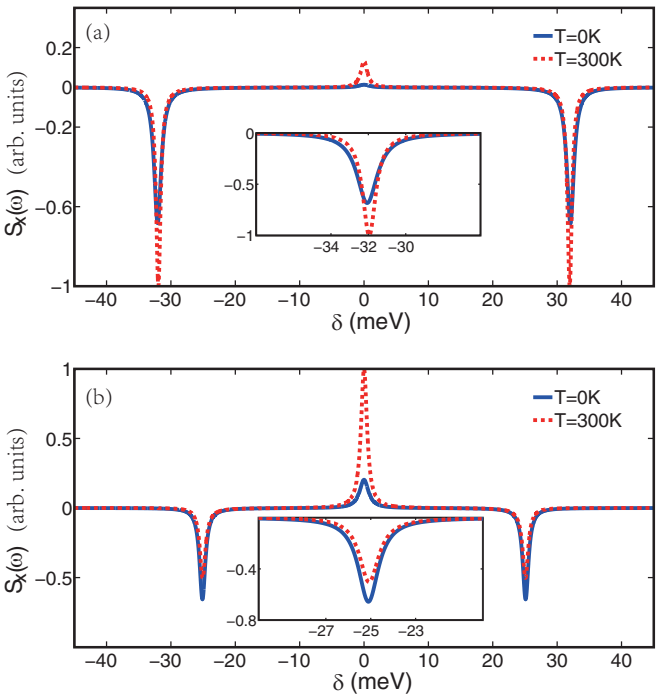

FIG. 6. Noise spectrum of the driven system for $\mu_f = 90$ meV, $\Omega = 20$ meV, $d = 10$ nm, and (a) $\gamma_0 = 5$ μeV and $\Delta = 25$ meV or (b) $\gamma_0 = 0.1$ meV and $\Delta = -15$ meV. The solid blue line and the dashed red line are used to highlight different environmental temperatures: the former represents zero temperature; the latter, room temperature.

In Fig. 6 we investigate the influence of the environmental temperature on squeezing. The Fermi energy and Rabi frequency are taken to be 90 and 20 meV, respectively. Figure 6(a) displays the spectrum for the case where the dephasing rate is $\gamma_0 = 5$ μeV and the QD detuning is 25 meV. It is obvious that squeezing at room temperature (dashed red line) is stronger than that at zero temperature (solid blue line). The relative illustrations are given below. First, for the parameters that we choose, the population differences $\langle\tilde{\sigma}_z\rangle_{ss}$ at both temperatures are close to each other and approximately take the minimum value -1. Then the main factor that influences the strength of squeezing lies in the strength of the reservoir-assisted decay process, which is proportioned to the LDOS around the graphene's surface. It is clear through Eq. (20) that an increase in the decay rate will cause a decrease in the squeezing amplitude, with the other parameters remaining unchanged. Thus for such special circumstances, owing to the destructive effect of an increase in the environmental temperature on the QD-graphene coupling, squeezing at room temperature will be stronger. Figure 6(b) displays the case for $\gamma_0 = 0.1$ meV and $\Delta = -15$ meV. It is clearly shown that as a response to the increase in the dephasing rate, the central peak of the resonance fluorescence increases, while the sidebands suffer a decrease, indicating that the squeezing becomes weaker. Differently from the former case, the imbalance in the population distribution is more prominent for zero environmental temperature, thus strong squeezing can be generated.

IV. TOTAL NORMAL-ORDER VARIANCES OF THE FLUORESCENCE FIELD

Measurement of the quadrature squeezing spectrum requires the emitted field to be first frequency filtered and then homodyned with a strong local oscillator field [70]. Practically, squeezing can also be detected in terms of the total normal-ordered variances of the phase quadratures in an alternative experimental scheme, where the total radiation field and the local oscillator are directly homodyned without first frequency filtering [71]. In the following we focus on the quadrature fluctuation of the radiation field, which can be derived by integrating the noise spectrum over all frequencies, yielding [72]

$$\langle :(\Delta E_s)^2: \rangle = \frac{\langle :\left(\Delta E_x\right)^2: \rangle}{\psi} = 1 + \langle \hat{\sigma}_z \rangle_{ss} - 4\langle \hat{\sigma}_- \rangle_{ss}^2, \quad (21)$$

where the quantity $\langle :(\Delta E_s)^2: \rangle$ represents the in-phase quadrature fluctuation scaled by the normalizing constant [73] ψ, while negative values indicate squeezing in the fluorescence field. Especially, the maximum squeezing can be achieved when it takes the value $-1/4$. Starting from Eq. (21), after transforming the QD operators into dressed-state formations, one can obtain the squeezing conditions: $(\langle\tilde{\sigma}_{--}\rangle_{ss} - \alpha^2)/\langle\tilde{\sigma}_{--}\rangle_{ss}(\langle\tilde{\sigma}_{--}\rangle_{ss} - 1) < 8\beta^2\alpha^2/(\beta^2 - \alpha^2)$ for positive detuning and $(\langle\tilde{\sigma}_{--}\rangle_{ss} - \alpha^2)/\langle\tilde{\sigma}_{--}\rangle_{ss}(\langle\tilde{\sigma}_{--}\rangle_{ss} - 1) > 8\beta^2\alpha^2/(\beta^2 - \alpha^2)$ for negative detuning. As suggested by the steady-state solutions, the appearance of squeezing will give rise to features controlled by $\Gamma_+ \gg \Gamma_-$ (or $\Gamma_- \gg \Gamma_+$). That is, the driven system should be mostly populated in the upper or lower dressed state. It has been previously shown that this imbalanced population distribution originates from a discrepancy in the LDOSs at different frequencies, which is characterized by a Lorentzian-like curve. Thus the total normal-order variances of the phase quadrature can be modified by tuning the experimental parameters.

Figure 7 shows the scaled quadrature fluctuation as a function of the chemical potential for pump conditions $\Delta = 10$ meV and $\Omega = 20$ meV. The dephasing rate is taken to be 5 μeV and the QD-graphene distance is 10 nm. It is clear that for both temperatures, squeezing of the fluorescence field appears when the Fermi energy is around 0.1 eV. Then the squeezing reaches its maximum value and gradually declines, finally disappearing at a Fermi energy near 0.39 eV. Note that squeezing can be generated for some energy values below 0.05 eV at zero temperature, whereas no squeezing occurs at room temperature. This phenomenon can be understood by analyzing the modes of the graphene-supported SPF, which has been done by Mikhailov *et al.* [74]. It was pointed out that in the low-THz frequency region where the interband transition is blocked, graphene can support both s-polarized and p-polarized surface modes. However, only one kind of surface mode can be excited for a specific excitation frequency. In the present system, the dipole momentum is assumed to be perpendicular to the graphene sheet, which indicates that only the p-polarized mode can be excited. When one transition channel is located in the frequency region where only the s-polarized mode can be supported (corresponding to the transition frequency $\omega_l \pm \bar{\Omega}$), the population will be distributed unevenly between the two dressed states owing to the suppression of the transition channel, and thus squeezing can be observed. With increasing Fermi energy, the resonant frequency of the SPF suffers blue shifts and gradually moves towards the frequency $\omega_l + \bar{\Omega}$. In this circumstance, the driven system couples much more strongly with the SPF modes around frequency $\omega_l + \bar{\Omega}$ rather than the modes around $\omega_l - \bar{\Omega}$, and there exists a huge discrepancy between the decay rates Γ_+ and Γ_-. Squeezing of the fluorescence radiation field can be observed when the Fermi energy is higher than 0.09 eV, while the maximum squeezing reaches -0.2 at zero environmental temperature. In the meantime, for the room-temperature case the enhanced intraband scattering broadens the SPF dispersion curve, which indicates a decline in the strength of QD-graphene coupling. Thus the difference in decay rates between two transition channels is decreased, and the maximum squeezing suffers a decrease. Additionally, the difference between decay rates shows a sharp decline for Fermi energies higher than 0.39 eV. As a result, squeezing disappears due to the destruction of the imbalanced populations.

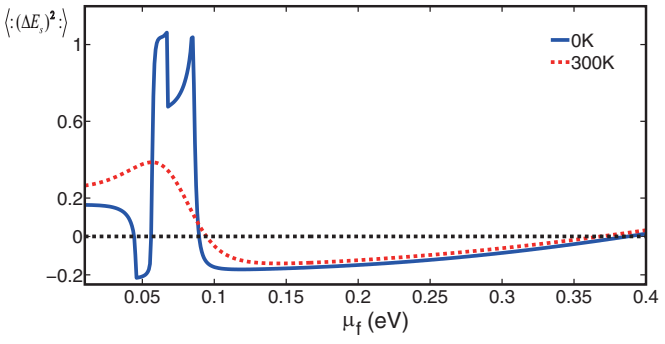

FIG. 7. Scaled quadrature fluctuation of resonance fluorescence vs the Fermi energy of graphene, for $d = 10$ nm, $\Omega = 20$ meV, $\Delta = 10$ meV, and $\gamma_0 = 5$ μeV; both the zero-temperature (solid blue line) and the room-temperature (dashed red line) cases are considered.

It is obvious in Fig. 7 that squeezing of the resonance fluorescence can be achieved by tuning the Fermi energy of graphene. However, squeezing can also be adjusted by tuning the pump field. Figure 8 provides a global view of the variation of $\langle :(\Delta E_s)^2: \rangle$ with the detuning Δ and Rabi frequency Ω at room temperature, and the decay rates of two symmetrical transition channels are also plotted to gain insight into the generation of squeezing. The Fermi energy and dephasing rate are chosen to be 0.1 eV and 5 μeV, respectively. As Figs. 8(a) and 8(b) depict, the decay rates vary with the laser intensity and the QD detuning, and the maximum values can be obtained when one transition channel of the dressed QD is resonantly coupled to the SPF. For negative QD detunings and high Rabi frequencies, the transition frequencies of the dressed QD tend to be distributed symmetrically on both sides of the resonant SPF frequency, which results in a diminishment of the population difference. When the pump frequency is lower than the excitation frequency, the transition corresponding to the frequency $\omega_l + \bar{\Omega}$ can be resonantly tuned with the SPF while the other channel is off-resonant, and thus a large discrepancy in the decay rates can be generated. As predicted, it is easy to produce strong squeezing with positive detunings, with the maximum squeezing reaching -0.2. Morever, it is also shown

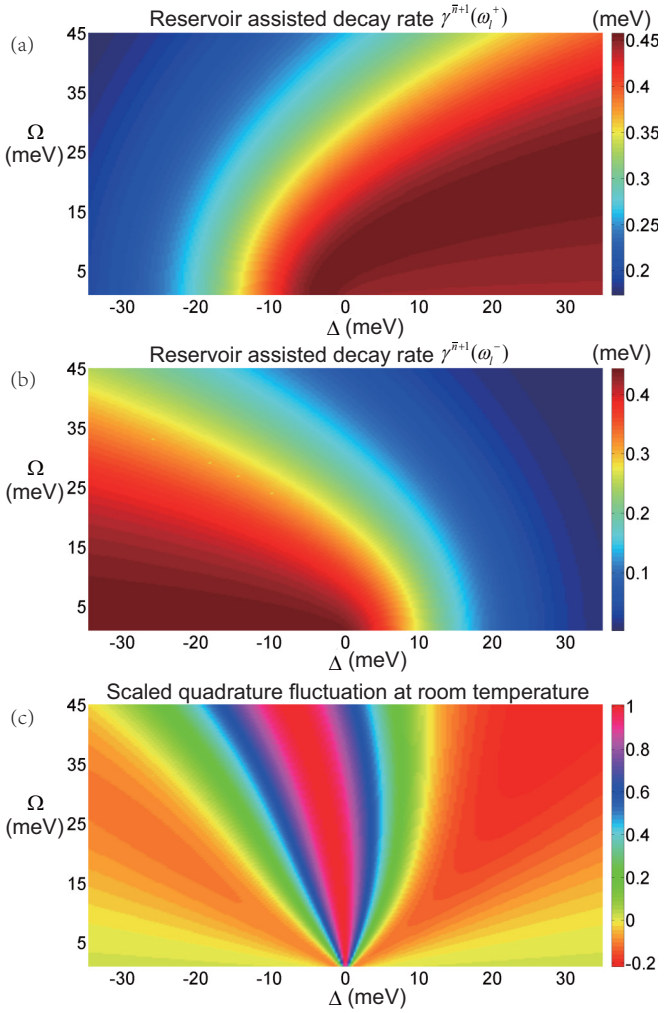

FIG. 8. Reservoir-assisted decay rates and the scaled quadrature fluctuation vs the QD detuning and Rabi frequency, for $\mu_f = 120$ meV, $\gamma_0 = 5$ μeV, and $T = 300$ K. (a) The decay rate $\gamma^{\bar{n}+1}(\omega_l^+)$, which corresponds to the transition channel $|+\rangle \to |-\rangle$. (b) The decay rate $\gamma^{\bar{n}+1}(\omega_l^-)$, which corresponds to the symmetrical transition channel $|-\rangle \to |+\rangle$. (c) Total normal-order invariance of in-phase quadrature.

in the figures that although a large discrepancy in the decay rates exists, squeezing cannot be generated when the Rabi frequency is much lower than the detuning. It can be understood that for low Rabi frequencies, the QD decouples from the pump laser and interacts only with the SPF modes on the graphene.

So far, the basic mechanism for the generation of squeezing in resonance fluorescence has been investigated. It has been shown that squeezing of the radiation field can be adjusted by tuning the parameters of either the graphene or the pump laser. The dispersion relation of the SPF on the surface of graphene has been illustrated by introduction of the Purcell factor. It is clear that an imbalanced decay process corresponding to the transition frequencies $\omega_l \pm \bar{\Omega}$ is important in the generation of squeezing. However, dephasing may have a destructive effect on the squeezing. Then it is found that by placing the QD closer to the graphene sheet, the increase in the coupling strength can overcome this issue, where squeezing can also be obtained for a high dephasing rate. Finally, the influences of the Fermi energy, QD detuning, and Rabi frequency on squeezing are studied. The results indicate that squeezing can be enhanced by tuning the intensity or the central frequency of the pump laser. Generally, a rising environmental temperature requires more restricted conditions for the generation of squeezing.

V. CONCLUSION

In this paper, we study the squeezing properties of the spectrum emitted by a laser-driven QD coupled to the SPF mode on the surface of graphene. The Lorentzian-shaped response of surface modes is shown through investigation of the Purcell factor. We find that the coupling strength between the QD and the SPF can be affected by the position of the QD and the environmental temperature. Then the master equation is derived and the noise spectrum is investigated. For off-resonant excitation ($\Delta \neq 0$), the noise spectrum of the in-phase quadrature exhibits two-mode squeezing at the Rabi sideband frequencies. The influences of dephasing, QD-graphene distance, and environmental temperature on squeezing are also studied. According to the analytical form of the noise spectrum and the steady-state solutions of the QD operators, the numerical results can be understood physically. It is shown that an increase in the dephasing rate precludes the generation of squeezing, while squeezing can be enhanced by placing the QD closer to the graphene sheet. Research on the total normal-ordered invariance indicates that in the strong QD-SPF coupling region, even at room temperature, squeezing can be produced and greatly enhanced by reasonably tuning the intensity and central frequency of the pump laser.

ACKNOWLEDGMENTS

This work was supported by the National Natural Science Foundation of China (Grants No. 61275123 and No. 11474119) and the National Basic Research Program of China (Grant No. 2012CB921602).

APPENDIX A: THE MASTER EQUATION AND OPTICAL BLOCH EQUATIONS FOR THE QUANTUM DOT

The master equation for the reduced density operator, in the frame of rotation with the pump frequency and transformation into the dressed-state basis, turns out to be

$$\begin{aligned}\frac{d\rho}{dt} =& \frac{1}{i\hbar}[\tilde{H}_0,\rho] + \frac{1}{2}\Gamma_-\mathcal{L}_{+-} + \frac{1}{2}\Gamma_+\mathcal{L}_{-+} + \frac{1}{8}(2\Gamma_p - \Gamma_i)\mathcal{L}_{zz} + \frac{1}{4}\alpha\beta(\beta^2-\alpha^2)\gamma_0(\mathcal{L}_{z-} + \mathcal{L}_{-z} + \text{H.c.}) \\ &+ i[\beta^4 P^{\bar{n}+1}(\omega_l^-) - \alpha^4 P^{\bar{n}}(\omega_l^+)][\tilde{\sigma}_-\tilde{\sigma}_+,\rho] + i[\alpha^4 P^{\bar{n}+1}(\omega_l^+) - \beta^4 P^{\bar{n}}(\omega_l^-)][\tilde{\sigma}_+\tilde{\sigma}_-,\rho] - [M(\bar{\Omega})\tilde{\sigma}_+\rho\tilde{\sigma}_+ + \text{H.c.}] \\ &+ \left[\sum_{j=1,2}\left(F_j^0[\tilde{\sigma}_-,\tilde{\sigma}_z^{(j-1)}\rho\tilde{\sigma}_z^{(2-j)}] + F_j[(-1)^{j-1}\bar{\Omega}][\tilde{\sigma}_-^{(2-j)}\rho\tilde{\sigma}_-^{(j-1)},\tilde{\sigma}_z]\right) + \text{H.c.}\right]. \end{aligned} \tag{A1}$$

In the above equation, $\tilde{H}_0 = \frac{\hbar\bar{\Omega}}{2}\tilde{\sigma}_z$ is the Hamiltonian of the driven QD in the dressed-state basis, the operator $\mathcal{L}_{mn} = 2\tilde{\sigma}_m\rho\tilde{\sigma}_n - \tilde{\sigma}_n\tilde{\sigma}_m\rho - \rho\tilde{\sigma}_n\tilde{\sigma}_m$ $(m,n = +, -, z)$, the dephasing process of the QD has been taken into account, and the coefficients in the master equation can be derived through the functions given below:

$$F_j^0 = \pi\alpha\beta\left\{\alpha^{2(2-j)}\beta^{2(j-1)}\gamma^{\bar{n}+1}(\omega_l) - \alpha^{2(j-1)}\beta^{2(2-j)}\gamma^{\bar{n}}(\omega_l) + \frac{i(-1)^{j-1}}{\pi}[P^{\bar{n}+1}(\omega_l) + P^{\bar{n}}(\omega_l)]\right\}, \tag{A2}$$

$$F_j(\eta) = \pi\alpha\beta\left\{\alpha^{2(2-j)}\beta^{2(j-1)}\left[\gamma^{\bar{n}+1}(\omega_l+\eta) + \frac{i(-1)^{2-j}}{\pi}P^{\bar{n}+1}(\omega_l+\eta)\right] - \alpha^{2(j-1)}\beta^{2(2-j)}\left[\gamma^{\bar{n}}(\omega_l-\eta) + \frac{i(-1)^{j-1}}{\pi}P^{\bar{n}}(\omega_l-\eta)\right]\right\}, \tag{A3}$$

$$M(\bar{\Omega}) = \pi\alpha^2\beta^2\left\{\gamma^{\bar{n}+1}(\omega_l^+) + \gamma^{\bar{n}+1}(\omega_l^-) + \gamma^{\bar{n}}(\omega_l^+) + \gamma^{\bar{n}}(\omega_l^-) + \frac{i}{\pi}[P^{\bar{n}+1}(\omega_l^+) - P^{\bar{n}+1}(\omega_l^-) + P^{\bar{n}}(\omega_l^+) - P^{\bar{n}}(\omega_l^-)]\right\}. \tag{A4}$$

It can be seen through Eq. (A1) that both the reservoir and the dephasing processes have impacts on the dynamics of the dressed QD, and the terms $\frac{1}{2}\Gamma_-\mathcal{L}_{+-}$, $\frac{1}{2}\Gamma_+\mathcal{L}_{-+}$, and $\frac{1}{8}(2\Gamma_p - \Gamma_i)\mathcal{L}_{zz}$ contribute to the Bloch equations under the secular approximation. Additionally, the other terms in the master equation, which are modulated by the pump laser and the reservoir, revise the behavior of the dressed QD when the secular approximation becomes illegal. Aside from the reservoir-assisted decay rates [$\gamma^{\bar{n}+1}(\omega)$ or $\gamma^{\bar{n}}(\omega)$; $\omega = \omega_l^-, \omega_l$, and ω_l^+], the coefficients $P^{\bar{n}+1}(\omega)$ and $P^{\bar{n}}(\omega)$ will also exist as the principal parts of integrals, which denote the energy shifts of the corresponding QD levels and have the following forms:

$$P^{\bar{n}}(\eta) = \mathcal{P}\int_0^\infty \frac{\gamma^{\bar{n}}(\omega)}{\omega-\eta}d\omega,$$
$$P^{\bar{n}+1}(\eta) = \mathcal{P}\int_0^\infty \frac{\gamma^{\bar{n}+1}(\omega)}{\omega-\eta}d\omega. \tag{A5}$$

The principal parts, which are shown in Eq. (A5), can be calculated numerically by use of the Kramers-Kronig relation of the Green function [51]. Through the master equation above, the corresponding Bloch equations can be derived after straightforward calculations, with explicit expressions

$$\langle\dot{\tilde{\sigma}}_+\rangle = c_1\langle\tilde{\sigma}_+\rangle + c_2\langle\tilde{\sigma}_-\rangle + c_3\langle\tilde{\sigma}_z\rangle + d_1, \tag{A6}$$

$$\langle\dot{\tilde{\sigma}}_-\rangle = c_1^*\langle\tilde{\sigma}_-\rangle + c_2^*\langle\tilde{\sigma}_+\rangle + c_3^*\langle\tilde{\sigma}_z\rangle + d_1^*, \tag{A7}$$

$$\langle\dot{\tilde{\sigma}}_z\rangle = c_4\langle\tilde{\sigma}_+\rangle + c_4^*\langle\tilde{\sigma}_-\rangle + c_5\langle\tilde{\sigma}_z\rangle + d_2, \tag{A8}$$

where the parameters in the above Bloch equations can be expressed with the combinations of QD decay rates and coefficients defined in Eqs. (A2)–(A4), and take the forms

$$c_1 = -\Gamma_p + i\Omega_p, \tag{A9}$$

$$c_2 = -M(\bar{\Omega})^* + \alpha^2\beta^2\gamma_0, \tag{A10}$$

$$c_3 = F_1(\bar{\Omega}) - F_2(-\bar{\Omega}) + \alpha\beta(\beta^2-\alpha^2)\gamma_0/2, \tag{A11}$$

$$c_4 = 2\left(F_1^0 - F_2^0\right)^* + \alpha\beta(\beta^2-\alpha^2)\gamma_0, \tag{A12}$$

$$c_5 = -\Gamma_i, \tag{A13}$$

$$d_1 = F_1(\bar{\Omega}) + F_2(-\bar{\Omega}) + F_1^0 + F_2^0, \tag{A14}$$

$$d_2 = \Gamma'. \tag{A15}$$

It is clear through Eqs. (A6)–(A8) that the expectation values $\langle\tilde{\sigma}_+\rangle$, $\langle\tilde{\sigma}_-\rangle$, and $\langle\tilde{\sigma}_z\rangle$ relate to each other during the evolution. In the strong-pump limit where the secular approximation is valid, the analytical form of Bloch equations can be deduced through the simplified master equation [dropping the rapidly varying terms and neglecting the principal parts in Eq. (A1)]. In this circumstance, the energy shifts $\Omega_p \approx \bar{\Omega}$ and the dynamical properties of the expectation values are determined only by the polarization decay rate Γ_p or population inversion decay rate Γ_i. As a result, the expectation values decouple from each other and evolve separately, where the analytical expressions are given in Eqs. (14)–(16) and summarized to further our understanding of the behavior of the dressed QD.

APPENDIX B: NUMERICAL APPROACH OF THE NOISE SPECTRUM RADIATED BY THE DRESSED QUANTUM DOT

The noise spectrum of the dressed QD, after transformation into the dressed-state basis, can be rewritten as

$$\begin{aligned}S_x(\omega) = \mathrm{Re}\int_0^\infty d\tau\cos(\Delta\omega\tau)\lim_{t\to\infty}\big[&2\alpha^2\beta^2\langle\tilde{\sigma}_z(t+\tau),\tilde{\sigma}_z(t)\rangle \\ &+ 2\beta\alpha^3\langle\tilde{\sigma}_z(t+\tau),\tilde{\sigma}_-(t)\rangle - 2\beta^3\alpha\langle\tilde{\sigma}_z(t+\tau),\tilde{\sigma}_+(t)\rangle \\ &+ (\alpha^4-\alpha^2\beta^2)\langle\tilde{\sigma}_+(t+\tau),\tilde{\sigma}_-(t)\rangle + (\beta^4-\beta^2\alpha^2) \\ &\times\langle\tilde{\sigma}_+(t+\tau),\tilde{\sigma}_+(t)\rangle + (\beta\alpha^3-\beta^3\alpha) \\ &\times\langle\tilde{\sigma}_+(t+\tau),\tilde{\sigma}_z(t)\rangle + (\beta^4-\alpha^2\beta^2) \\ &\times\langle\tilde{\sigma}_-(t+\tau),\tilde{\sigma}_+(t)\rangle + (\alpha^4-\alpha^2\beta^2) \\ &\times\langle\tilde{\sigma}_-(t+\tau),\tilde{\sigma}_-(t)\rangle + (\beta\alpha^3-\beta^3\alpha) \\ &\times\langle\tilde{\sigma}_-(t+\tau),\tilde{\sigma}_z(t)\rangle\big].\end{aligned} \tag{B1}$$

In the strong-pump region where the Bloch equations can be described by Eqs. (14)–(16), most of the correlation functions

in Eq. (B1) vanish and do not contribute to the spectrum. In this circumstance, the steady-state solutions of the QD operators are easy to derive and the explicit expression of the noise spectrum is given in Eq. (20). Generally, in order to make our result confidential, we use Eqs. (A6)–(A8) to evaluate the radiation spectrum of the dressed QD. Then by use of the quantum regression theory, the noise spectrum can be derived and represented in terms of the sum of steady-state fluctuations of the QD operators,

$$\begin{aligned} S_x(\omega) = \frac{1}{2}\mathrm{Re}\sum_{s=s_1,s_2}\{&A[(\beta^4-\beta^2\alpha^2)\langle\tilde{\sigma}_+,\tilde{\sigma}_+\rangle_{ss}+(\alpha^4-\alpha^2\beta^2)\\ &\times\langle\tilde{\sigma}_+,\tilde{\sigma}_-\rangle_{ss}+(\beta\alpha^3-\beta^3\alpha)\langle\tilde{\sigma}_+,\tilde{\sigma}_z\rangle_{ss}]\\ &+B[(\beta^4-\alpha^2\beta^2)\langle\tilde{\sigma}_-,\tilde{\sigma}_+\rangle_{ss}+(\alpha^4-\alpha^2\beta^2)\\ &\times\langle\tilde{\sigma}_-,\tilde{\sigma}_-\rangle_{ss}+(\beta\alpha^3-\beta^3\alpha)\langle\tilde{\sigma}_-,\tilde{\sigma}_z\rangle_{ss}]\\ &+C[2\alpha^2\beta^2\langle\tilde{\sigma}_z,\tilde{\sigma}_z\rangle_{ss}+2\beta\alpha^3\langle\tilde{\sigma}_z,\tilde{\sigma}_-\rangle_{ss}-2\beta^3\alpha\\ &\times\langle\tilde{\sigma}_z,\tilde{\sigma}_+\rangle_{ss}]\}/D_2, \end{aligned} \tag{B2}$$

$$\begin{aligned} A = {}& c_4c_3^*+c_1^*c_5+c_2^*c_4^*-c_2^*c_5-c_4^*c_3^*-c_4c_1^*\\ &+(c_2^*+c_4-c_1^*-c_5)s+s^2, \end{aligned} \tag{B3}$$

$$\begin{aligned} B = {}& c_1c_5+c_4^*c_3+c_4c_2-c_4c_3-c_2c_5-c_1c_4^*\\ &+(c_2+c_4^*-c_1-c_5)s+s^2, \end{aligned} \tag{B4}$$

$$\begin{aligned} C = {}& c_2^*c_3+c_2c_3^*+c_1c_1^*-c_1c_3^*-c_1^*c_3-c_2^*c_2\\ &+(c_3^*+c_3-c_1-c_1^*)s+s^2, \end{aligned} \tag{B5}$$

$$\begin{aligned} D_2 = {}& c_4c_1^*c_3+c_1c_4^*c_3^*+c_2^*c_2c_5-c_2^*c_4^*c_3-c_4c_2c_3^*\\ &-c_1c_1^*c_5+(c_1c_1^*+c_1c_5+c_1^*c_5-c_2^*c_2-c_4c_3\\ &-c_4^*c_3^*)s-(c_1+c_1^*+c_5)s^2+s^3, \end{aligned} \tag{B6}$$

where $s_1 = i(\omega-\omega_l)$ and $s_2 = -i(\omega-\omega_l)$, and the definitions of elements in the coefficients are given in Eqs. (A9)–(A15). Morever, the steady-state fluctuations in Eq. (B2) can be rewritten in the form of the steady-state solutions of the expectation values, which appears to be

$$\begin{aligned} \langle\tilde{\sigma}_+,\tilde{\sigma}_+\rangle_{ss} &= -\langle\tilde{\sigma}_+\rangle_{ss}^2,\\ \langle\tilde{\sigma}_+,\tilde{\sigma}_-\rangle_{ss} &= (1+\langle\tilde{\sigma}_z\rangle_{ss}-2\langle\tilde{\sigma}_+\rangle_{ss}\langle\tilde{\sigma}_-\rangle_{ss})/2,\\ \langle\tilde{\sigma}_+,\tilde{\sigma}_z\rangle_{ss} &= -\langle\tilde{\sigma}_+\rangle_{ss}(1+\langle\tilde{\sigma}_z\rangle_{ss}),\\ \langle\tilde{\sigma}_-,\tilde{\sigma}_+\rangle_{ss} &= (1-\langle\tilde{\sigma}_z\rangle_{ss}-2\langle\tilde{\sigma}_+\rangle_{ss}\langle\tilde{\sigma}_-\rangle_{ss})/2,\\ \langle\tilde{\sigma}_-,\tilde{\sigma}_-\rangle_{ss} &= -\langle\tilde{\sigma}_-\rangle_{ss}^2,\\ \langle\tilde{\sigma}_-,\tilde{\sigma}_z\rangle_{ss} &= \langle\tilde{\sigma}_-\rangle_{ss}(1-\langle\tilde{\sigma}_z\rangle_{ss}),\\ \langle\tilde{\sigma}_z,\tilde{\sigma}_+\rangle_{ss} &= \langle\tilde{\sigma}_+\rangle_{ss}(1-\langle\tilde{\sigma}_z\rangle_{ss}),\\ \langle\tilde{\sigma}_z,\tilde{\sigma}_-\rangle_{ss} &= -\langle\tilde{\sigma}_-\rangle_{ss}(1+\langle\tilde{\sigma}_z\rangle_{ss}),\\ \langle\tilde{\sigma}_z,\tilde{\sigma}_z\rangle_{ss} &= 1-\langle\tilde{\sigma}_z\rangle_{ss}^2. \end{aligned} \tag{B7}$$

The steady-state expectation values of the QD operators $\langle\tilde{\sigma}_+\rangle_{ss}$, $\langle\tilde{\sigma}_-\rangle_{ss}$, and $\langle\tilde{\sigma}_z\rangle_{ss}$, which determine the steady-state fluctuations as shown in Eq. (B7), can be easily obtained from Eqs. (A6)–(A8).

[1] A. K. Geim and K. S. Novoselov, Nat. Mater. **6**, 183 (2007).
[2] A. H. Castro Neto, F. Guinea, N. M. R. Peres, K. S. Novoselov, and A. K. Geim, Rev. Mod. Phys. **81**, 109 (2009).
[3] F. Bonaccorso, Z. Sun, T. Hasan, and A. C. Ferrari, Nat. Photon. **4**, 611 (2010).
[4] L. Chirolli, M. Polini, V. Giovannetti, and A. H. MacDonald, Phys. Rev. Lett. **109**, 267404 (2012).
[5] M. J. Paul, J. L. Tomaino, J. W. Kevek, T. DeBorde, Z. J. Thompson, E. D. Minot, and Y. S. Lee, Appl. Phys. Lett. **101**, 091109 (2012).
[6] P. A. Huidobro, A. Y. Nikitin, C. González-Ballestero, L. Martín-Moreno, and F. J. García-Vidal, Phys. Rev. B **85**, 155438 (2012).
[7] S. F. Shi, T. T. Tang, B. Zeng, L. Ju, Q. Zhou, A. Zettl, and F. Wang, Nano Lett. **14**, 1578 (2014).
[8] N. Rouhi, S. Capdevila, D. Jain, K. Zand, Y. Y. Wang, E. Brown, L. Jofre, and P. Burke, Nano Res. **5**, 667 (2012).
[9] A. J. Frenzel, C. H. Lui, Y. C. Shin, J. Kong, and N. Gedik, Phys. Rev. Lett. **113**, 056602 (2014).
[10] G. W. Hanson, J. Appl. Phys. **103**, 064302 (2008).
[11] M. Jablan, H. Buljan, and M. Soljačić, Phys. Rev. B **80**, 245435 (2009).
[12] H. Yan, X. Li, B. Chandra, G. Tulevski, Y. Wu, M. Freitag, W. Zhu, P. Avouris, and F. Xia, Nat. Nanotech. **7**, 330 (2012).
[13] Q. L. Bao and K. P. Loh, ACS Nano **6**, 3677 (2012).
[14] D. R. Andersen, J. Opt. Soc. Am. B **27**, 818 (2010).
[15] J. S. Gomez-Diaz, C. Moldovan, S. Capdevila, J. Romeu, L. S. Bernard, A. Magrez, A. M. Lonescu, and J. Perruisseau-Carrier, Nat. Commun. **6**, 6334 (2015).
[16] V. P. Gusynin, S. G. Sharapov, and J. P. Carbotte, J. Phys. Condens. Matter **19**, 026222 (2007).
[17] N. Sule, K. J. Willis, S. C. Hagness, and I. Knezevic, Phys. Rev. B **90**, 045431 (2014).
[18] F. H. L. Koppens, D. E. Chang, and F. J. García de Abajo, Nano Lett. **11**, 3370 (2011).
[19] L. M. Malard, K. F. Mak, A. H. Castro Neto, N. M. R. Peres, and T. F. Heinz, New J. Phys. **15**, 015009 (2013).
[20] Z. Q. Li, E. A. Henriksen, Z. Jiang, Z. Hao, M. C. Martin, P. Kim, H. L. Stormer, and D. N. Basov, Nat. Phys. **4**, 532 (2008).
[21] J. M. Dawlaty, S. Shivaraman, J. Strait, P. George, M. Chandrashekhar, F. Rana, M. G. Spencer, D. Verksler, and Y. Q. Chen, Appl. Phys. Lett. **93**, 131905 (2008).
[22] V. P. Gusynin, S. G. Sharapov, and J. P. Carbotte, Phys. Rev. B **75**, 165407 (2007).
[23] E. H. Hwang, S. Adam, and S. Das Sarma, Phys. Rev. Lett. **98**, 186806 (2007).
[24] T. O. Wehling, K. S. Novoselov, S. V. Morozov, E. E. Vdovin, M. I. Katsnelson, A. K. Geim, and A. I. Lichtenstein, Nano Lett. **8**, 173 (2008).

[25] E. V. Gorbar, V. P. Gusynin, A. B. Kuzmenko, and S. G. Sharapov, Phys. Rev. B **86**, 075414 (2012).

[26] F. Wang, Y. B. Zhang, C. S. Tian, C. Girit, A. Zettl, M. Crommie, and Y. R. Shen, Science **320**, 206 (2008).

[27] L. Ren, Q. Zhang, J. Yao, Z. Z. Sun, R. Kaneko, Z. Yan, S. Nanot, Z. Jin, I. Kawayama, M. Tonouchi, J. M. Tour, and J. Kono, Nano Lett. **12**, 3711 (2012).

[28] K. I. Bolotin, K. J. Sikes, Z. Jiang, M. Klima, G. Fudenberg, J. Hone, P. Kim, and H. L. Stormer, Solid State Commun. **146**, 351 (2008).

[29] S. D. Sarma, S. Adam, E. H. Hwang, and E. Rossi, Rev. Mod. Phys. **83**, 407 (2011).

[30] L. Ju, B. S. Geng, J. Horng, C. Girit, M. Martin, Z. Hao, H. A. Bechtel, X. G. Liang, A. Zettl, Y. R. Shen, and F. Wang, Nat. Nanotech. **6**, 630 (2011).

[31] A. Vakil and N. Engheta, Science **332**, 1291 (2011).

[32] J. Chen, M. Badioli, P. Alonso-González, S. Thongrattanasiri, F. Huth, J. Osmond, M. Spasenović, A. Centeno, A. Pesquera, P. Godignon, A. Z. Elorza, N. Camara, F. J. García de Abajo, R. Hillenbrand, and F. H. L. Koppens, Nature **487**, 77 (2012).

[33] B. R. Mollow, Phys. Rev. **188**, 1969 (1969).

[34] H. J. Kimble and L. Mandel, Phys. Rev. A **13**, 2123 (1976).

[35] D. F. Walls and P. Zoller, Phys. Rev. Lett. **47**, 709 (1981).

[36] H. Grote, K. Danzmann, K. L. Dooley, R. Schnabel, J. Slutsky, and H. Vahlbruch, Phys. Rev. Lett. **110**, 181101 (2013).

[37] S. Takeda, T. Mizuta, M. Fuwa, H. Yonezawa, P. van Loock, and A. Furusawa, Phys. Rev. A **88**, 042327 (2013).

[38] U. L. Andersen, J. S. Neergaard-Nielsen, P. van Loock, and A. Furusawa, Nat. Phys. **11**, 713 (2015).

[39] C. H. H. Schulte, J. Hansom, A. E. Jones, C. Matthiesen, C. L. Gall, and M. Atatüre, Nature **525**, 222 (2015).

[40] L. L. Jin, M. Marcovei, S. Q. Gong, C. H. Keitel, and J. Evers, Opt. Commun. **283**, 790 (2010).

[41] C. Eichler, D. Bozyigit, C. Lang, M. Baur, L. Steffen, J. M. Fink, S. Filipp, and A. Wallraff, Phys. Rev. Lett. **107**, 113601 (2011).

[42] R. Guzmán, J. C. Retamal, E. Solano, and N. Zagury, Phys. Rev. Lett. **96**, 010502 (2006).

[43] D. Martín-Cano, H. R. Haakh, K. Murr, and M. Agio, Phys. Rev. Lett. **113**, 263605 (2014).

[44] G. X. Li, S. P. Wu, and J. P. Zhu, J. Opt. Soc. Am. B **27**, 1634 (2010).

[45] P. Grünwald and W. Vogel, Phys. Rev. A **88**, 023837 (2013).

[46] S. Y. Gao and F. L. Li, Opt. Commun. **266**, 231 (2006).

[47] R. Jacob, S. Winnerl, M. Fehrenbacher, J. Bhattacharyya, H. Schneider, M. T. Wenzel, H-G. V. Ribbeck, L. M. Eng, P. Atkinson, O. G. Schmidt, and M. Helm, Nano Lett. **12**, 4336 (2012).

[48] E. A. Zibik, T. Grange, B. A. Carpenter, N. E. Porter, R. Ferreira, G. Bastard, D. Stehr, S. Winnerl, M. Helm, H. Y. Liu, M. S. Skolnick, and L. R. Wilson, Nat. Mater. **8**, 803 (2009).

[49] Y. Zhang, K. Shibata, N. Nagai, C. Ndebeka-Bandou, G. Bastard, and K. Hirakawa, Nano Lett. **15**, 1166 (2015).

[50] B. Huttner and S. M. Barnett, Phys. Rev. A **46**, 4306 (1992).

[51] T. Gruner and D. G. Welsch, Phys. Rev. A **53**, 1818 (1996).

[52] H. T. Dung, S. Y. Buhmann, L. Knöll, D. G. Welsch, S. Scheel, and J. Kästel, Phys. Rev. A **68**, 043816 (2003).

[53] M. S. Tomaš, Phys. Rev. A **51**, 2545 (1995).

[54] H. W. Liang, S. C. Ruan, M. Zhang, H. Su, and I. L. Li, Appl. Phys. Lett. **107**, 091602 (2015).

[55] P. Y. Chen, J. Soric, Y. R. Padooru, H. M. Bernety, A. B. Yakovlev, and A. Alù, New J. Phys. **15**, 123029 (2013).

[56] N. M. R. Peres, F. Guinea, and A. H. Castro Neto, Phys. Rev. B **73**, 125411 (2006).

[57] W. Takayuki, F. Tetsuya, Y. Yuhei, A. B. T. Stephane, S. Akira, A. D. Alexander, Y. A. Vladimir, M. Vladimir, R. Victor, and O. Taiichi, New J. Phys. **15**, 075003 (2013).

[58] Y. W. Tan, Y. Zhang, K. Bolotin, Y. Zhao, S. Adam, E. H. Hwang, S. Das Sarma, H. L. Stormer, and P. Kim, Phys. Rev. Lett. **99**, 246803 (2007).

[59] H. Choi, F. Borondics, D. A. Siegel, S. Y. Zhou, M. C. Martin, A. Lanzara, and R. A. Kaindl, Appl. Phys. Lett. **94**, 172102 (2009).

[60] C. Van Vlack, P. T. Kristensen, and S. Hughes, Phys. Rev. B **85**, 075303 (2012).

[61] D. E. Chang, A. S. Sørensen, P. R. Hemmer, and M. D. Lukin, Phys. Rev. B **76**, 035420 (2007).

[62] X. D. Zeng, G. X. Li, Y. P. Yang, and S. Y. Zhu, Phys. Rev. A **86**, 033819 (2012).

[63] W. C. Chew, *Waves and Fields in Inhomogeneous Media* (IEEE, New York, 1995).

[64] A. Archambault, T. V. Teperik, F. Marquier, and J. J. Greffet, Phys. Rev. B **79**, 195414 (2009).

[65] M. O. Scully and M. S. Zubairy, *Quantum Optics* (Cambridge University Press, Cambridge, UK, 1997).

[66] M. Teich, D. R. Stephan, S. Winnerl, H. Schneider, L. R. Wilson, and M. Helm, Appl. Phys. Lett. **103**, 252110 (2013).

[67] M. J. Collett, D. F. Walls, and J. Zoller, Opt. Commun. **52**, 145 (1984).

[68] M. Cerbu, M. A. Macovei, and G. X. Li, Phys. Rev. A **89**, 013837 (2014).

[69] H. P. Breuer and F. Petruccione, *The Theory of Open Quantum Systems* (Oxford University Press, New York, 2002).

[70] H. Z. Zhao, Z. H. Lu, A. M. Bacon, L. J. Wang, and J. E. Thomas, Phys. Rev. A **57**, 1427 (1998).

[71] E. Shchukin and W. Vogel, Phys. Rev. Lett. **96**, 200403 (2006).

[72] D. F. Walls, Nature **306**, 141 (1983).

[73] B. J. Dalton, Z. Ficek, and P. L. Knight, Phys. Rev. A **50**, 2646 (1994).

[74] S. A. Mikhailov and K. Ziegler, Phys. Rev. Lett. **99**, 016803 (2007).